Transient Stability Analysis for Grid-Forming Inverters Transitioning from Islanded to Grid-Connected Mode

Liu, Teng; Wang, Xiongfei; Liu, Fangcheng; Xin, Kai; Liu, Yunfeng

Published in:
IEEE Open Journal of Power Electronics

DOI (link to publication from Publisher):
10.1109/OJPEL.2022.3189801

Publication date:
2022

Document Version
Publisher's PDF, also known as Version of record

IEEE Open Journal of
Power Electronics

Received 19 May 2022; revised 20 June 2022; accepted 5 July 2022. Date of publication 11 July 2022; date of current version 21 July 2022. The review of this article was arranged by Associate Editor Cheng Wang.

Digital Object Identifier 10.1109/OJPEL.2022.3189801

Transient Stability Analysis for Grid-Forming Inverters Transitioning from Islanded to Grid-Connected Mode

TENG LIU [1] (Member, IEEE), XIONGFEI WANG [1] (Senior Member, IEEE), FANGCHENG LIU[2] (Senior Member, IEEE), KAI XIN[2], AND YUNFENG LIU[2]

[1]Department of Energy, Aalborg University, 9220 Aalborg, Denmark
[2]Huawei Technologies Co Ltd, Shanghai 201206, China

CORRESPONDING AUTHOR: XIONGFEI WANG (e-mail: xwa@energy.aau.dk)

ABSTRACT This paper addresses the transient stability of grid-forming (GFM) inverters when transitioning from the islanded to grid-connected mode. It is revealed that the reconnection of the GFM inverters to the main grid can be equivalent to a step change of the active power reference, whose impact is closely related with the local load, active power reference of GFM inverter, and short-circuit ratio (SCR) of the grid. Such equivalent disturbance may cause GFM inverters lose the synchronism with the grid. To avoid loss of synchronization, the existence of equilibria of GFM inverter after reconnecting it with the grid is examined, considering the varying SCR. Then, the parametric effects of power controllers on the transient stability are characterized by using phase portraits, which shed clear insights into the controller design for reliably reconnecting GFM inverters with grid. Lastly, all the theoretical findings are confirmed by experimental tests.

INDEX TERMS Grid-forming inverters, grid-connected mode, islanded mode, local load, resynchronization, transient stability.

I. INTRODUCTION

Inverter-based resources (IBRs) are increasingly deployed to accelerate the green transition of electric power grids [1]. To accommodate the proliferation and even 100% IBRs, the grid-forming (GFM) technology emerges as a promising solution [2], [3]. By directly regulating the magnitude and frequency of the output voltage, the GFM inverter is controlled as a voltage source behind a reactance [4], [5].

Thanks to the voltage-source nature, GFM inverters are able to operate stably with a low short-circuit ratio (SCR) in the grid-connected (GC) mode [6], and naturally operate in the islanded (IS) mode to maintain the system voltage and frequency [7]. Hence, GFM inverters can get rid of the control reconfiguration during the transition between the GC and IS modes [8]. Yet, to avoid undesired overcurrent when GFM inverters transitioning from the IS mode to GC mode, the magnitude, frequency, and phase angle differences between the inverter output voltage and grid voltage should meet the requirement imposed by IEEE Std. 1547-2018 [9]. Hence, resynchronizing GFM inverters with the grid is mandatory for a smooth transition from the IS mode to GC mode [10].

The resynchronization methods used with GFM inverters can be categorized into two groups. The first group is based on the phase-locked loop (PLL). In [11], two PLLs are used to obtain the phase angle difference between the inverter output voltage and grid voltage. Then, the phase angle difference is regulated by a proportional-integral (PI) controller, whose output is added to the reference frequency generated by the *P-f* droop control, to achieve zero phase angle difference. In [12], only one PLL is used to detect the phase angle of grid voltage, which is further used with the *abc/dq*-transformation of inverter output voltage. Thus, a zero phase difference can be realized by regulating the obtained *q*-axis output voltage to zero. A similar idea is already reported in [13], where the PLL is used to obtain the phase angle of grid voltage, which is compared with the internal phase of GFM inverter and the phase difference is used to adjust the frequency reference of droop controller for resynchronization.

The second group belongs to the PLL-free resynchronization schemes, where the phase angle difference is obtained without using the PLL. A virtual impedance-based resynchronization method is reported in [14]. The main idea is to emulate a virtual impedance between the GFM inverter and grid, and the current flowing through the virtual impedance is controlled to zero to resynchronize the inverter with the grid. Another way to obtain the phase angle difference is through the cross-product of the grid voltage and inverter voltage vectors [15], [16], and a zero phase angle difference is achieved by adjusting the reference frequency generated from the active power control loop.

Generally speaking, once the output voltage of GFM inverter is resynchronized with the grid voltage, a seamless transition from the IS to GC mode can be expected. However, as will be revealed later in this work, the GFM inverter may still lose its synchronism with the main grid after the reconnection with grid, and such loss of synchronism (LOS) is attributed to the transient instability of GFM inverters [17].

Recently, the transient stability of GFM inverters is attracting considerable attention. The transient stability of GFM inverter with the first-order power synchronization control (PSC) is analyzed in [18]. It is shown that the PSC-GFM inverter can maintain the synchronism as long as the equilibrium points (EPs) exist after large disturbances. In contrast, when the second-order PSC, e.g., the virtual synchronous generator (VSG) control or the *P-f* droop control with a low-pass filter (LPF), is applied with the GFM inverter for inertia emulation, the transient stability would be deteriorated with a large inertia, and the GFM inverter may lose its synchronism even when the EPs exist [19]. The impact of *Q-V* droop control on the transient stability of GFM inverter is analyzed in [20], which reveals that the *Q-V* droop control can adversely affect the transient stability. Besides, the impacts of inner control loops, e.g., the single-loop voltage magnitude control and current limiting control, on the transient stability of GFM inverters have also been reported in recent studies [21]–[23]. Moreover, the transient stability of microgrids operating in the IS mode has also been investigated [24], and the voltage angle deviations with respect to the angle of the center of inertia are used as a tool for transient stability assessment of multi-VSGs microgrid [25]. However, all those works focus on the transient stability of GFM inverters in either the GC or the IS mode, while little attention has been paid to the transient stability of GFM inverters transitioning between the GC and IS modes. Recently, through the simulation tests, the transient stability issues have been identified when the GFM inverters transition from the GC to IS mode, and it reveals that the local loads have a critical impact on the transient stability during the transition process [26], [27]. However, the transient stability in the transition of GFM inverters from the IS to GC mode still remains an open issue.

This paper thus attempts to bridge the gap by revealing the mechanism behind the LOS of GFM inverters in transitioning from the IS to GC mode. The main contributions of this paper are highlighted as follows.

- It is revealed that the reconnection of GFM inverters to the main grid can be equivalent to a step change of the active power reference, whose impact on the transient stability of GFM inverter after reconnection is highly dependent on the local load, the active power reference of GFM inverter, and the short-circuit ratio (SCR) of the grid.
- The existence of the EPs after the reconnection of GFM inverters to the grid is examined, considering the impact of varying SCR of the grid. It is found out that the decrease of SCR increases the risk of losing EPs, and hence, GFM inverters are prone to LOS when reconnecting to a weaker ac grid.
- The impact of the *Q-V* droop control is characterized through the phase portrait analysis. It is interestingly found that the impact of *Q-V* droop control is also dependent on the local load. When the local load demands more active power than that generated by GFM inverter, i.e., the active power is flowing from the grid to local load, the *Q-V* droop control enhances the transient stability of GFM inverter after reconnecting it with the grid. In contrast, when the grid-side active power flow reverses with the lower active power consumed by the local load, the *Q-V* droop control jeopardizes the transient stability after reconnecting GFM inverter with the grid.
- Further, the parametric effects of power controllers on the transient stability of GFM inverters in transitioning from the IS mode to GC mode are analyzed. It reveals that the parametric effect of PSC is independent on the direction of grid-side active power flow, whereas the effect of the *Q-V* droop coefficient is closely related with the direction of grid-side active power flow.

Lastly, all the theoretical findings are verified by experimental test results.

II. RESYNCHRONIZATION OF GFM INVERTERS

A. SYSTEM DESCRIPTION

Fig. 1 shows the single-line diagram of a three-phase GFM inverter with the local load. L_f and C_f denote the output *LC* filter of inverter. The local load connected to the ac bus is composed of the paralleled *RLC* components in this work. The main grid consists of an ideal voltage source v_g in series with an inductor L_g. v_{pcc} denotes the ac bus voltage. i_o and i_g are the output currents of the GFM inverter and the grid-side currents injected into the grid, respectively. The switch S_1 represents the static transfer switch (STS). When S_1 is closed, the GFM inverter operates in the GC mode. When S_1 is open, the GFM inverter operates in the IS mode, where v_s equals to v_g. Hence, v_s is detected for resynchronization with the grid, to ensure a smooth transition of GFM inverter from the IS to GC mode.

During abnormal condition of main grid, the GFM inverter is intentionally disconnected from the grid and supplies power to the local load. In the IS mode, the magnitude and frequency of v_{pcc} are determined by the GFM control scheme and local load. When the main grid is restored, the magnitude

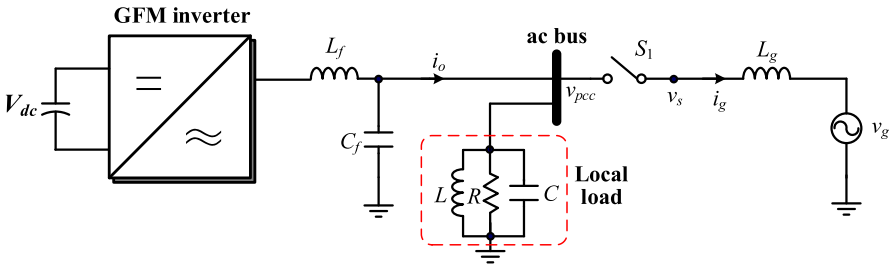

FIGURE 1. Single-line diagram of a three-phase GFM inverter with the paralleled *RLC* local load.

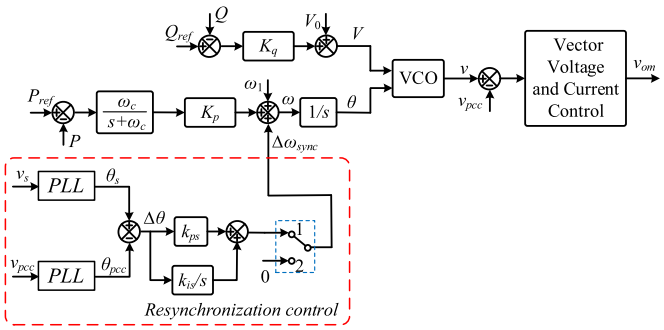

FIGURE 2. Control block diagram of the GFM inverter with the resynchronization control scheme, where the switch is in the position 1 for resynchronization with the grid, and in the position 2 after reconnecting inverter to the grid.

and frequency of v_{pcc} may deviate from those of v_s. If S_1 is directly closed, their magnitude and phase differences may cause undesired transient overcurrent tripping the inverter. According to IEEE Std. 1547-2018, the magnitude, frequency, and phase differences between v_{pcc} and v_s should satisfy the synchronization parameter limits before the reconnection of GFM inverters [9]. Therefore, before the closure of S_1, it is necessary to assure that v_{pcc} is in phase with v_s (i.e., v_g) for the seamless transition of GFM inverters from the IS to GC mode.

B. RESYNCHRONIZATION CONTROL SCHEME

The overall control structure of the GFM inverter is shown in Fig. 2. The outer reactive power loop adopts the conventional Q-V droop control in this work. Based on Fig. 2, the Q-V droop control generates the voltage magnitude reference V for the inner voltage control loop, whose control law is given by

$$V = K_q\left(Q_{ref} - Q\right) + V_0 \tag{1}$$

where K_q is the Q-V droop coefficient, V_0 is the rated voltage magnitude, and Q_{ref} is the reference value of the reactive power.

The second-order PSC is used with the outer active power loop, which is based on the P-f droop control with an LPF for the emulation of inertia and damping effects. The output of the active power loop dictates the reference of phase angle θ for the inner voltage loop. Then, V and θ are used by the voltage-controlled oscillator (VCO) to generate the voltage vector reference v for the ac bus voltage. To tightly regulate v_{pcc} to follow its reference, the inner voltage control employs the cascaded dual-loop vector voltage and current control [18], which finally generates the modulation voltage reference v_{om} for the pulsewidth modulation.

The resynchronization control scheme reported in [11] is used in this work to resynchronize v_{pcc} with v_s before the closure of S_1, whose control block diagram is shown in the red dashed box in Fig. 2. It is worth noting that other resynchronization methods can also be applied, while the transient instability issue of reconnecting GFM inverter to the grid is independent of the used resynchronization method, as will be explained in Section III.B.

From Fig. 2, the phase angles of v_{pcc} and v_s are obtained through two PLLs, respectively, and then their difference $\Delta\theta$ is fed into a PI controller, whose output $\Delta\omega_{sync}$ is added to the output of PSC to determine the angular frequency ω of the voltage reference. Thus, θ_{pcc} is equal to θ_s in the steady state, and an effective resynchronization is achieved.

The overall control law of the outer active power loop during the resynchronization process (i.e., before the closure of S_1) is given by

$$\theta = \frac{1}{s}\cdot\left[K_p\cdot\frac{\omega_c}{s+\omega_c}\cdot\left(P_{ref}-P\right)+\left(k_{ps}+\frac{k_{is}}{s}\right)\cdot\Delta\theta+\omega_1\right] \tag{2}$$

where K_p is the P-f droop coefficient, ω_c is the cut-off angular frequency of the LPF, and P_{ref} represents the active power reference. k_{ps} and k_{is} are the proportional and integral gains of the PI controller in the resynchronization control, respectively. ω_1 is the grid fundamental angular frequency. It is worth noting that the PI controller of the resynchronization control loop is only enabled during the resynchronization process and it must be deactivated after the closure of S_1 to allow power exchange between inverter and grid [11].

The effectiveness of the resynchronization control scheme is tested by the PSCAD/EMTDC simulation with the main system parameters listed in Table 1. The simulation waveforms during the transition from the IS to GC mode are presented in Fig. 3, where $L_g = 20$ mH and $P_{ref} = 1.2$ kW are selected in this test. Before $t = 1$ s, the GFM inverter operates in the IS mode supplying the power to the local load. Since the output frequency of GFM inverter is deviated from the grid frequency, there exists a phase angle difference between v_{pcc}

TABLE 1 Main System Parameters for Simulation and Experimental Tests

Item	Symbol	Value
Grid voltage (*l-g*, rms)	v_g	50 V
Grid fundamental frequency	f_1	50 Hz
Switching frequency	f_{sw}	10 kHz
Filter inductor	L_f	3 mH
Filter capacitor	C_f	15 μF
Grid-side inductor	L_g	24, 20, 6 mH
Resistor of *RLC* load	R	3 Ω
Inductor of *RLC* load	L	16 mH
Capacitor of *RLC* load	C	645 μF
Rated voltage magnitude	V_0	70.71 V
Active power reference	P_{ref}	1, 1.2, 2.8 kW
Reactive power reference	Q_{ref}	0 Var
P-f droop coefficient	K_p	$0.05\omega_1/P_{ref}$
Q-V droop coefficient	K_q	$0.10V_0/P_{ref}$

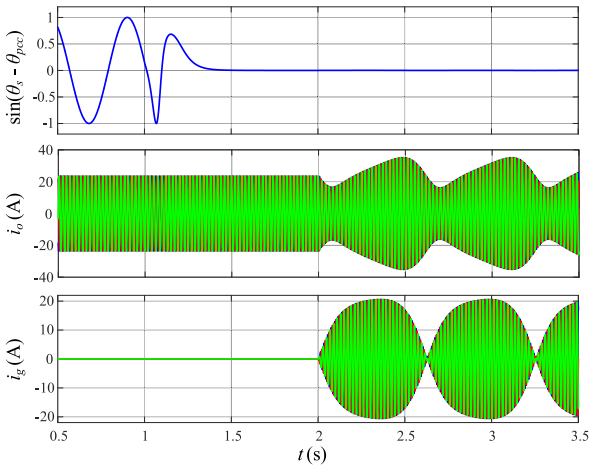

FIGURE 3. The simulation waveforms of the GFM inverter during the transition from the IS to GC mode. The resynchronization controller is enabled at $t = 1$ s and the STS S_1 is closed at $t = 2$ s.

and v_s. At $t = 1$ s, the resynchronization controller is activated to synchronize v_{pcc} with v_s. It is observed that the phase angle difference is regulated to zero around $t = 1.4$ s.

III. TRANSIENT INSTABILITY OF RECONNECTING GFM INVERTER WITH GRID

A. PHENOMENON OF LOSS OF SYNCHRONISM

As shown in Fig. 3, after v_{pcc} is in phase with v_s, the STS S_1 is closed at $t = 2$ s to reconnect GFM inverter with the grid. It is observed that an unexpected low-frequency oscillation arises, causing the failure of grid reconnection. Therefore, though the resynchronization is successfully achieved, the GFM inverter may still lose its synchronism with the main grid during the reconnection process. The mechanism behind this instability phenomenon is revealed in the following.

B. CAUSE OF LOSS OF SYNCHRONISM

First, possible disturbance that results in this instability issue should be identified. At the instant of grid reconnection, there are actually two dynamic actions. One is the closure of S_1, and

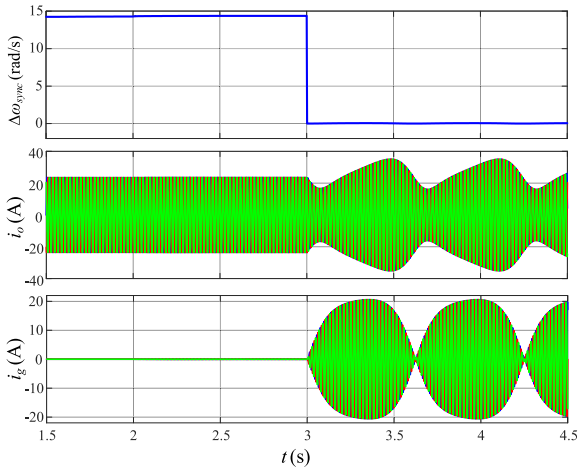

FIGURE 4. When the closure of S_1 happens at $t = 2$ s and the bypass of PI controller in the resynchronization control loop takes place at $t = 3$ s, the simulation waveforms of the GFM inverter during the transition from the IS to GC mode.

the other is the bypass of the PI controller of resynchronization control.

To figure out which one of the two actions plays a critical role in such instability phenomenon, these two actions are intentionally separated in the timeline. The resulted simulation waveforms are shown in Fig. 4, where the closure of S_1 happens at $t = 2$ s and the bypass of the PI controller takes place at $t = 3$ s. It is observed that, during $t = 2$ to 3 s, even though the GFM inverter with the local load are reconnected to the power grid, the entire system runs at the previous operating point in the resynchronization process, i.e., the GFM inverter only supplies the power to the local load, and there is no power injected into or extracted from the grid. This is because v_{pcc} and v_g have exactly the same magnitude and phase angle at $t = 2$ s, and this operating state will not be changed due to the integrator of the PI controller. Hence, the closure of S_1 will not disturb the system equilibria.

On the contrary, it is observed that the bypass of the PI controller at $t = 3$ s changes the system operating state, which leads to the power redistribution among the network. Hence, the disturbance that takes effect at the instant of grid reconnection is the bypass of PI controller in the resynchronization control loop, and such disturbance is inevitable for the purpose of the power exchange with the grid [11].

From the above discussion, it is figured out that the LOS of the GFM inverter in transitioning from the IS to GC mode is attributed to the bypass of resynchronization controller, which is mandatory for the power redistribution among the network. Therefore, this instability problem is independent of the used resynchronization control scheme, but related with the way of setting its output to zero. Directly setting the output of the PI controller to zero is studied in this work to satisfy the time requirement of the power redistribution after reconnecting the GFM inverter with the grid. Another point to be noted is that intentionally separate the closure of S_1 and the bypass of PI

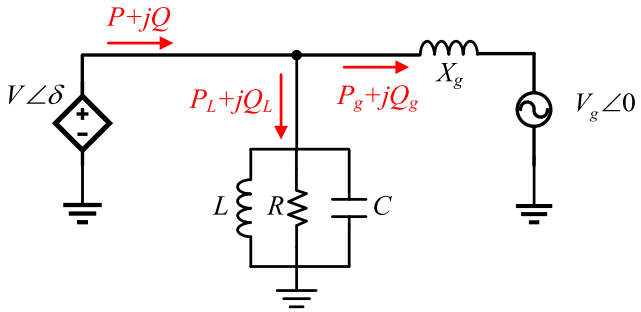

FIGURE 5. Steady-state system equivalent circuit in the grid-connected mode.

controller is only adopted to identify the disturbance after grid reconnection, while simultaneous occurrence of these two dynamic actions is applied for the following analyses.

C. MECHANISM OF LOSS OF SYNCHRONISM

Further, the mechanism behind the bypass of PI controller in the resynchronization control loop is analyzed. According to Fig. 2, the steady-state active power in the resynchronization process can be expressed by (3) with the assumption that the grid frequency is equal to ω_1.

$$K_p\left(P_{ref}-P\right)+\Delta\omega_{sync}=K_p\left(\underbrace{P_{ref}+\frac{\Delta\omega_{sync}}{K_p}}_{P_{refeq}}-P\right)=0 \tag{3}$$

Based on (3), the equivalent active power reference of the GFM inverter in the resynchronization process can be treated as P_{refeq}, which is equal to the steady-state active power consumed by the local load. When the resynchronization is achieved, v_{pcc} will have the same magnitude and phase angle with those of v_g. Hence, P_{refeq} can be calculated as

$$P_{refeq}=1.5\frac{V_g^2}{R} \tag{4}$$

where V_g is the magnitude of the grid voltage.

At the instant of grid reconnection, the bypass of PI controller is realized by setting $\Delta\omega_{sync}$ to zero. Based on (3), the equivalent active power reference will have a step change from P_{refeq} to P_{ref} with the zero setting of $\Delta\omega_{sync}$. Hence, the bypass of the PI controller can be further equivalent to a step change of the active power reference ΔP_{ref}, and its magnitude is calculated by $|P_{refeq}-P_{ref}|$. According to (4), it is found out that the magnitude of ΔP_{ref} is determined by the resistance of local load and the active power reference of GFM inverter.

After obtaining ΔP_{ref}, it is necessary to evaluate whether it is a small or large disturbance to the system. To this end, the way of obtaining the active power-angle curve, i.e., P - δ curve, is introduced first. Based on Fig. 1, the steady-state equivalent circuit of GFM inverter in the GC mode is shown in Fig. 5, where the phase angle of the grid voltage is taken as the reference angle. δ denotes the phase difference between v_{pcc} and v_g, which is also known as the power angle. P_L and Q_L are the active and reactive power of the local load, respectively. P_g and Q_g are the active and reactive power flowing into the main grid, respectively.

According to Fig. 5, the steady-state power flows of the system in the GC mode are given by

$$\begin{cases} P=P_L+P_g=\frac{3}{2}\cdot\frac{V^2}{R}+\frac{3}{2}\cdot\frac{V\cdot V_g}{X_g}\sin\delta \\ Q=Q_L+Q_g=\frac{3}{2}\cdot\frac{V^2}{R}\cdot Q_f\left(\frac{f_0}{f_1}-\frac{f_1}{f_0}\right)+\frac{3}{2}\cdot\frac{V^2-VV_g\cos\delta}{X_g} \end{cases} \tag{5}$$

where $X_g=2\pi f_1 L_g$, f_1 is the grid fundamental frequency, Q_f denotes the quality factor of the *RLC* load, and f_0 represents the resonant frequency of the *RLC* load. Q_f and f_0 can be calculated as

$$Q_f=R\cdot\sqrt{\frac{C}{L}}f_0=\frac{1}{2\pi\sqrt{LC}} \tag{6}$$

By substituting the reactive power equation in (5) into (1), the steady-state relationship between V and δ is solved as

$$V=\frac{n+\sqrt{n^2+6K_qX_g\left(1+\frac{X_gQ_fm}{R}\right)\left(K_qQ_{ref}+V_0\right)}}{3K_q\left(1+\frac{X_gQ_fm}{R}\right)}\triangleq g(\delta) \tag{7}$$

where

$$\begin{cases} m=\frac{f_0}{f_1}-\frac{f_1}{f_0} \\ n=1.5K_qV_g\cos\delta-X_g \end{cases} \tag{8}$$

Then, the relationship between P and δ can be obtained by substituting (7) into the active power equation in (5), which is given by

$$P=\frac{3}{2}\cdot\frac{g^2(\delta)}{R}+\frac{3}{2}\cdot\frac{g(\delta)\cdot V_g}{X_g}\sin\delta \tag{9}$$

Based on (9), the P - δ curve can be readily plotted under certain SCR of grid and local load conditions. Fig. 6 illustrates the P - δ curves under strong and weak grids, where the main system parameters except L_g in Table 1 are applied and $P_{ref}=1.2$ kW is selected. Different SCRs are emulated by varying L_g, where the SCR is calculated by

$$\mathrm{SCR}=\frac{3}{2}\cdot\frac{V_g^2}{X_gP_{ref}} \tag{10}$$

It is noted that the calculation of SCR in this work follows a general way without considering the impact of the local load. From Fig. 6, when the resynchronization is achieved, the GFM inverter initially operates at point ***o*** with $\delta=0$, which is exactly the intersection point between P_{refeq} and P - δ curves. When the STS S_1 is closed, the bypass of PI controller will make the operating point of the GFM inverter move from point ***o*** to the new EP, which is the intersection points between P_{ref} and P - δ curves.

Under the strong grid condition, i.e., SCR = 8, the GFM inverter will move from point ***o*** to point ***a'*** after the closure

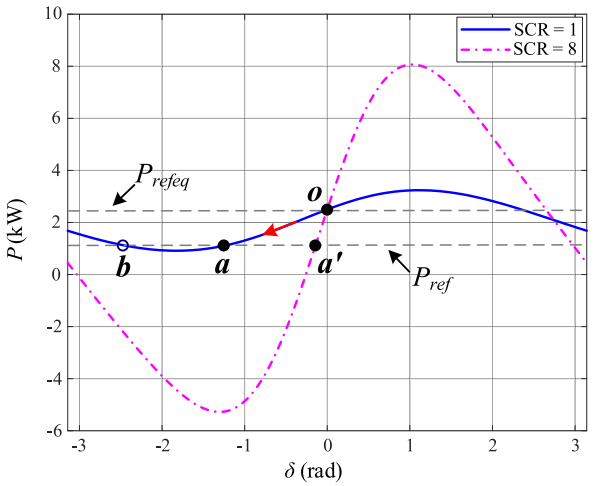

FIGURE 6. *P* - δ curves to show different impacts of equivalent disturbance under strong and weak grid conditions.

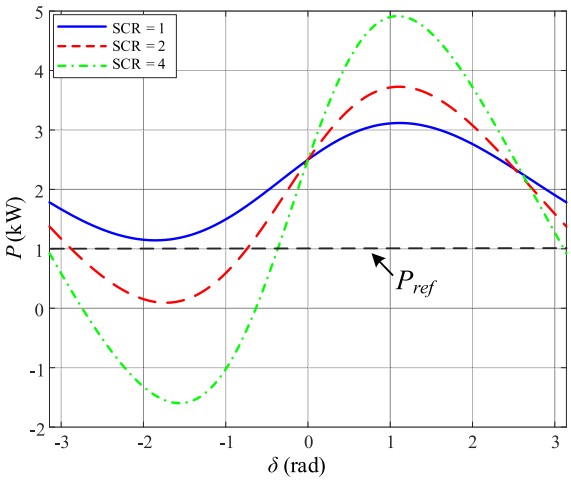

FIGURE 7. *P* - δ curves to analyze the impact of SCR on the existence of the EPs after grid reconnection.

of S_1. From the P - δ curve with SCR = 8, it is observed that P_{ref} is far away from the maximum active power transfer limit. Hence, the equivalent active power reference step change can be treated as a small disturbance to the reconnection of GFM inverter with a strong grid, where dynamics of such transition process is governed by the small-signal stability around EPs. In contrast, when the SCR is reduced to 1, it is clear that P_{ref} is close to the maximum active power transfer limit, which thus makes such equivalent step change become a large disturbance bringing the transient instability challenge to GFM inverters after the grid reconnection. From Fig. 6, there exist two intersection points between P_{ref} and P - δ curve. One is the stable EP ***a***, and the other is the unstable EP ***b***. The transient stability of GFM inverter is guaranteed only when δ finally converges to point ***a*** after the grid reconnection.

Therefore, it can be concluded that, whether the equivalent step change of active power reference ΔP_{ref} is a small or large disturbance to the grid-reconnection of GFM inverters is not only determined by the difference between P_{refeq} and P_{ref}, but also affected by the SCR of grid. Even if the magnitude of ΔP_{ref} is the same, it may cause a small disturbance in the strong grid condition, yet becomes a large disturbance if reconnecting GFM inverter to a weak grid. Since the small-signal stability under certain EPs of GFM inverters has been well documented in [17], this paper mainly focuses on the transient stability of GFM inverter during the transition from the IS to GC mode.

IV. TRANSIENT STABILITY ANALYSIS OF GFM INVERTERS AFTER GRID RECONNECTION

A. IMPACT OF SCR ON THE EXISTENCE OF EQUILIBRIUM POINTS

To ensure a stable transition of GFM inverter from the IS to GC mode, a necessary condition is that the GFM inverter system has EPs after the grid reconnection [18].

Based on (2), P will be equal to its reference value P_{ref} in the steady state after grid reconnection with the assumption that the grid frequency is ω_1. Consequently, the existence of the EPs can be easily predicted if there exist the intersection points between P_{ref} and the P - δ curve. Following the similar way to plot the P - δ curves in Figs. 6, 7 shows the P - δ curves to analyze the impact of SCR on the existence of EPs, where $P_{ref} = 1$ kW is used as an example.

From Fig. 7, it is observed that the GFM inverter has the EPs with SCR = 4. When the SCR is decreased to 2, P_{ref} will gradually approaches to the maximum active power transfer limit but still has the EPs with the P - δ curve. When SCR is further decreased to 1, there is no intersection point between P_{ref} and the P - δ curve, which indicates that the GFM inverter will lose its synchronism with the grid after the closure of S_1. Hence, the decrease of SCR would increase the risk of losing EPs, which implies that the GFM inverter is more prone to the LOS when it is reconnected to a weaker grid.

B. DYNAMIC MODEL OF GFM INVERTERS AFTER GRID RECONNECTION

Since the existence of EPs is only the necessary condition of transient stability, further nonlinear dynamic analysis is needed after reconnecting GFM inverter with the grid. Based on the principle of model reduction, the fast-timescale dynamics of the system are idealized when analyzing slow-timescale dynamics [28]. As the dynamic of inner voltage control loop is usually designed much faster than that of the outer power control loops, the inner voltage loop is idealized as a unity gain in the transient stability analysis, i.e., v_{pcc} tracks its reference v ideally [20].

According to Fig. 2 and considering $\theta_g = \omega_1 t$, the expression of δ is obtained as

$$\delta = \frac{1}{s} \cdot \left[K_p \cdot \frac{\omega_c}{s + \omega_c} \cdot \left(P_{ref} - P \right) + \Delta\omega_{sync} \right] \tag{11}$$

By applying the differentiator on both sides of (11), the dynamic behavior of δ is given by

$$\ddot{\delta} = -\omega_c \dot{\delta} + \omega_c \left[K_p \left(P_{ref} - P\right) + \Delta\omega_{sync}\right] + \Delta\dot{\omega}_{sync} \quad (12)$$

According to (12) and considering $\Delta\omega_{sync} = 0$ after grid reconnection, the dynamic behavior of δ is derived as

$$\frac{1}{\omega_c K_p}\ddot{\delta} = -\frac{1}{K_p}\dot{\delta} + P_{ref} - 1.5\frac{V^2}{R} - 1.5\frac{V \cdot V_g}{X_g}\sin\delta \quad (13)$$

By combining (1) with the reactive power equation, the dynamic of V is expressed as

$$V = K_q \times \left\{Q_{ref} - \frac{3}{2}\cdot\left[\frac{V^2 - V\cdot V_g\cos\delta}{X_g} + \frac{V^2}{R}\cdot Q_f\left(\frac{\omega_0}{\omega} - \frac{\omega}{\omega_0}\right)\right]\right\} + V_0 \quad (14)$$

where $\omega = \dot{\theta} = \dot{\delta} + \omega_1$. Based on (14), the dynamic relationship between V and δ can be given by (15), shown at the bottom of this page.

Finally, the dynamic behavior of δ with the consideration of the Q-V droop control can be derived by substituting (15) into (13), whose expression is given by

$$\frac{1}{\omega_c K_p}\ddot{\delta} = -\frac{1}{K_p}\dot{\delta} + P_{ref} - 1.5\frac{h^2(\delta)}{R} - 1.5\frac{V_g \cdot h(\delta)}{X_g}\sin\delta \quad (16)$$

C. IMPACT OF Q-V DROOP CONTROL ON THE TRANSIENT STABILITY

Based on (16), the phase portrait, which illustrates the $\dot{\delta}$-δ curve, is applied for the system transient stability assessment [29]. The Matlab command "ode45" is adopted to solve (16) with the initial value (0, 0) when resynchronization is attained. It is known that the active power will be extracted from the grid after reconnection when the local load demands more active power than that generated by GFM inverter, i.e., $P_{ref} < P_{refeq}$, and the grid-side active power flow reverses with the lower active power consumed by the local load, i.e., $P_{ref} > P_{refeq}$. Hence, the direction of grid-side active power flow can be emulated by setting different P_{ref}. The obtained phase portraits with the Q-V droop control are shown in Fig. 8, where the main system parameters listed in Table 1 are applied, and $L_g = 20$ mH is selected. To clearly show the impact of the Q-V droop control on the transient stability, the phase portraits with a constant voltage magnitude control, i.e., $V = V_0 = 1.0$ p.u., are also plotted in Fig. 8 for a comparison.

From Fig. 8(a), it is observed that, with a constant V, the trajectory starts from the initial steady-state point ***o*** and finally converges to a new stable EP ***c***, indicating that the system

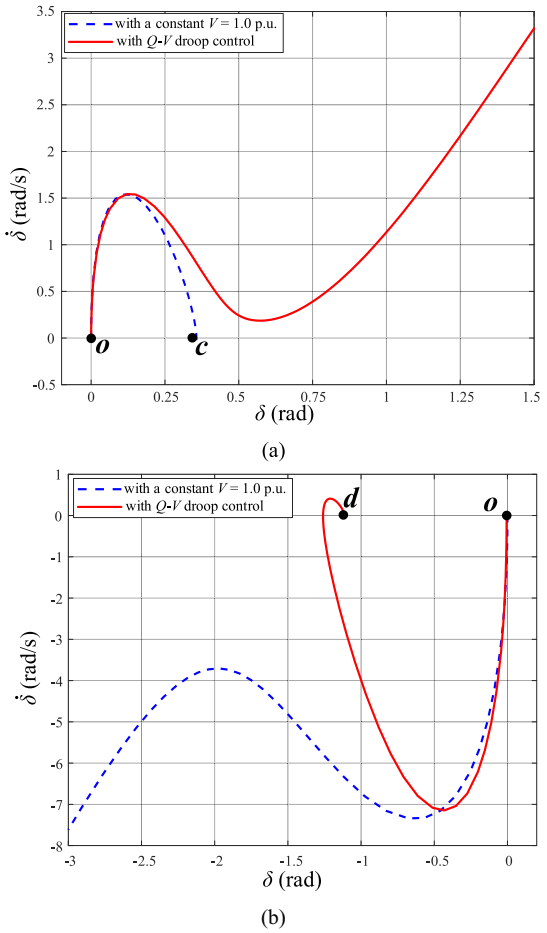

FIGURE 8. Phase portraits of the GFM inverter with and without considering the *Q-V* droop control when (a) the active power is injected into the grid after reconnection, (b) Active power is extracted from the grid after reconnection.

transient stability is assured after the grid reconnection. Since $\delta > 0$ during the dynamic process, it is known that the active power is injected into the grid in this condition. However, when the Q-V droop control is included, the GFM inverter cannot keep synchronism with the grid due to the divergence of δ. Hence, from Fig. 8(a), it is concluded that the Q-V droop control tends to deteriorate the system transient stability. This finding coincides with the existing conclusion reported in [20]. Nevertheless, it is interesting to note that, this conclusion is no longer valid for the phase portraits presented in Fig. 8(b). From Fig. 8(b), it can be observed that, when the active power is extracted from the grid after the reconnection ($\delta < 0$), the case with a constant V cannot achieve a stable transition of GFM inverter from the IS to GC mode. On the contrary, with

$$V = \frac{1.5K_qV_g\cos\delta - X_g + \sqrt{\left(1.5K_qV_g\cos\delta - X_g\right)^2 + 6K_qX_g\left[1 + \frac{X_gQ_f}{R}\cdot\left(\frac{\omega_0}{\delta+\omega_1} - \frac{\dot{\delta}+\omega_1}{\omega_0}\right)\right]\left(K_qQ_{ref} + V_0\right)}}{3K_q\left[1 + \frac{X_gQ_f}{R}\cdot\left(\frac{\omega_0}{\delta+\omega_1} - \frac{\dot{\delta}+\omega_1}{\omega_0}\right)\right]} \triangleq h(\delta) \quad (15)$$

the help of the *Q*-*V* droop control, the GFM inverter keeps the transient stability with the trajectory of δ converging to a new stable EP.

Based on the above analysis, it is found that the impact of the *Q*-*V* droop control on the transient stability depends on the direction of grid-side active power flow. When the active power is extracted from the grid after the reconnection, the *Q*-*V* droop control can enhance the transient stability. By contrast, when the active power is injected into the grid after the reconnection, the *Q*-*V* droop control jeopardizes the transient stability.

The physical insights of the above conclusions can be further qualitatively explained by the P - δ curves with and without the *Q*-*V* droop control, which are illustrated in Fig. 9. In the range of $\delta > 0$, i.e., when the active power is injected into the grid, it is observed that, the P - δ curve with the *Q*-*V* droop control has poorer active power transfer capability, in comparison with the P - δ curve with a constant V. Consequently, when δ moves from the initial point ***o*** to a new stable EP after the reconnection, the acceleration area is increased and the deceleration area is decreased, which, according to the equal area criterion [30], indicates that the *Q*-*V* droop control jeopardizes the transient stability. In contrast, the opposite phenomenon can be observed in the range of $\delta < 0$, where the P - δ curve with the *Q*-*V* droop control has smaller acceleration area and larger deceleration area compared to the P - δ curve with a constant V. In this scenario, the transient stability is enhanced by the *Q*-*V* droop control. It should be mentioned that the above descriptions are merely approximated elaboration, since the P - δ curve with the *Q*-*V* droop control during dynamic process is always changing with the change of V, and the dynamic of V is determined by (15). Even so, these P - δ curves can, to some extent, reveal the physical insights of the above findings, and they are also match with rigorous phase portrait-based transient stability analysis presented in Fig. 8.

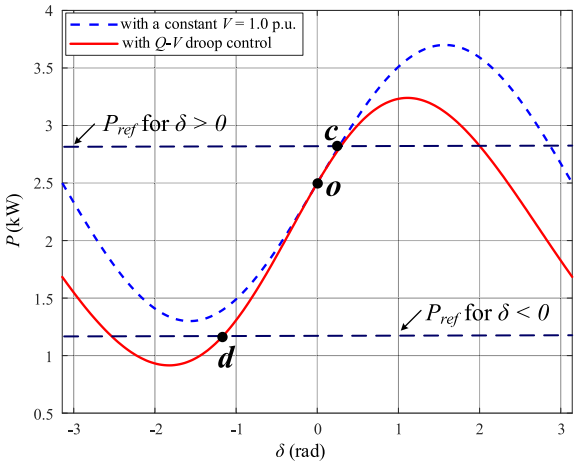

FIGURE 9. ***P*** **-** δ **curve with and without considering the *Q*-*V* droop control to qualitatively explain the relationship between the *Q*-*V* droop impact on the transient stability and the grid-side active power flow direction.**

D. PARAMETRIC EFFECTS OF POWER CONTROLLERS ON THE TRANSIENT STABILITY

Next, the parametric effects of the power controllers on the transient stability during the transition process are investigated. The controller parameters related with the PSC are analyzed first, where the cutoff frequency f_c of the LPF is taken as an example. By varying f_c and keeping other parameters fixed, the corresponding phase portraits with different directions of grid-side active power flow are plotted in Fig. 10. Fig. 10(a) shows the cases in which the active power is extracted from the grid after the reconnection. From Fig. 10(a), when $f_c = 10$ Hz, the phase portrait starts from the initial point ***o***, and then moves to a new stable EP ***d*** indicating a transient stable transition after the closure of S_1. Besides, compared to the case with $f_c = 2$ Hz, an overdamped dynamic response is achieved. In contrast, when $f_c = 0.5$ Hz, the phase portrait finally diverges leading to an unstable transition from islanded to grid-connected mode. The same impact of f_c on the transient stability can also be observed from Fig. 10(b), where the active power is injected into the grid after the reconnection. Hence, it is concluded that the decrease of f_c deteriorates the transient stability, regardless of the grid-side active power flowing direction. The effect of *P*-*f* droop coefficient can also be analyzed in a similar way, where the obtained phase portraits with different K_p are shown in Fig. 11. It is observed that the impact of K_p on the transient stability during transition process is independent on the grid-side active power flow direction, and the decrease of K_p leads to a more damped system with the enhancement of transient stability.

Further, the controller parameter related with the *Q*-*V* droop control, i.e., the droop coefficient K_q, is analyzed, and the corresponding phase portraits are presented in Fig. 12. It is observed from Fig. 12(a) that, the increase of K_q can enhance the transient stability when the active power is extracted from the grid after reconnection. On the contrary, from Fig. 12(b), the increase of K_q jeopardizes the transient stability when the active power is injected into the grid.

A brief summary of parametric effects of the power control loops to enhance the transient stability during transition process is listed in Table 2. It is concluded that the transient stability can be enhanced by decreasing K_p or increasing f_c in the PSC loop, regardless of the grid-side active power flowing direction after the grid reconnection. As for K_q in the *Q*-*V* droop control, its impact on the transient stability is dependent on the grid-side active power flowing direction. The decrease of K_q when $\delta > 0$ or the increase of K_q when $\delta < 0$ can enhance the system transient stability.

E. IMPACT OF INDUCTIVE AND CAPACITIVE LOAD ON THE TRANSIENT STABILITY

Based on (5), the reactive power consumed by the *RCL* load is rewritten in (17). From (17), when $f_0 > f_1$, Q_L will be positive. According to the power flow direction defined in Fig. 5, the *RLC* load absorbs the reactive power in this case indicating an inductive load. In contrast, when $f_0 < f_1$, Q_L will be negative

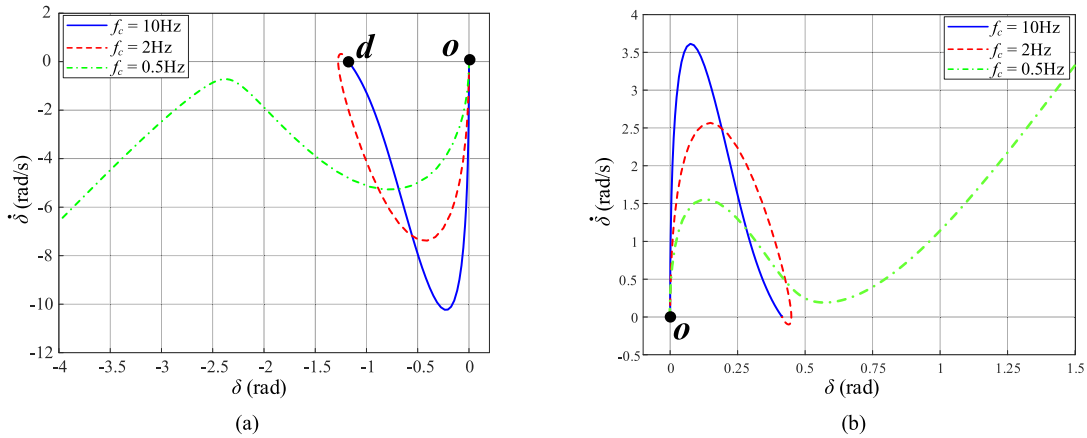

FIGURE 10. Phase portraits of the GFM inverter with different LPF cutoff frequency f_c of the PSC when (a) the active power is extracted from the grid after reconnection, (b) the active power is injected into the grid after reconnection.

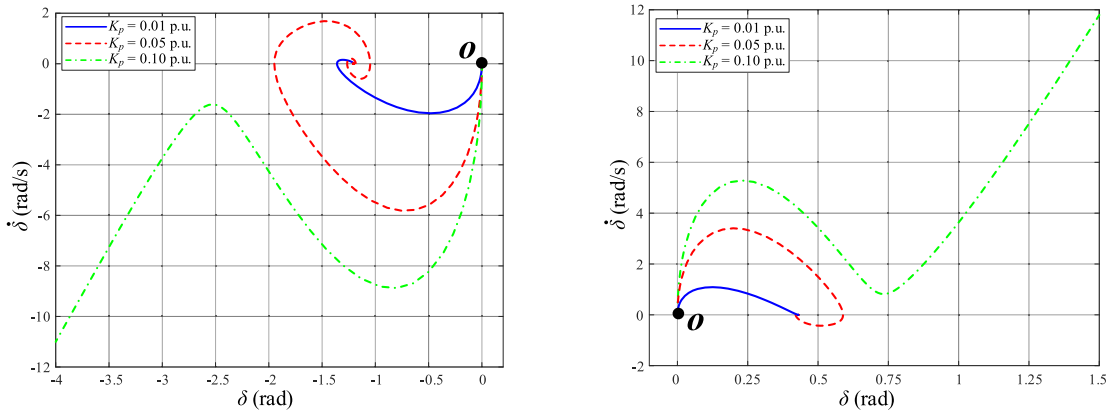

FIGURE 11. Phase portraits of the GFM inverter with different droop coefficients K_P of the PSC when (a) the active power is extracted from the grid after reconnection, (b) the active power is injected into the grid after reconnection.

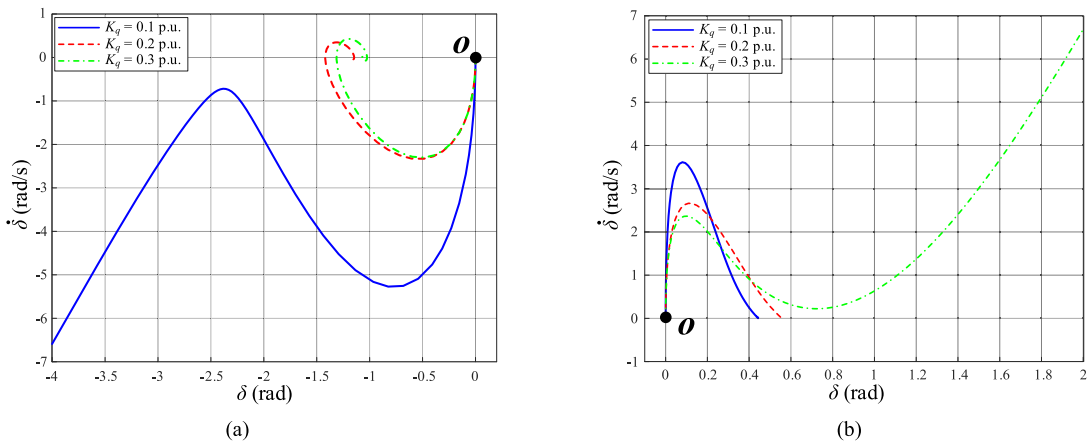

FIGURE 12. Phase portraits of the GFM inverter with different *Q-V* droop coefficient K_q when (a) the active power is extracted from the grid after reconnection, (b) the active power is injected into the grid after reconnection.

TABLE 2 Parametric Effects of Power Control Loops to Enhance Transient Stability

Controller parameters	Parametric effects to enhance transient stability	
	When $\delta > 0$	When $\delta < 0$
P-f droop coefficient K_p in the PSC loop	↓	↓
LPF cut-off frequency f_c in the PSC loop	↑	↑
Q-V droop coefficient K_q	↓	↑

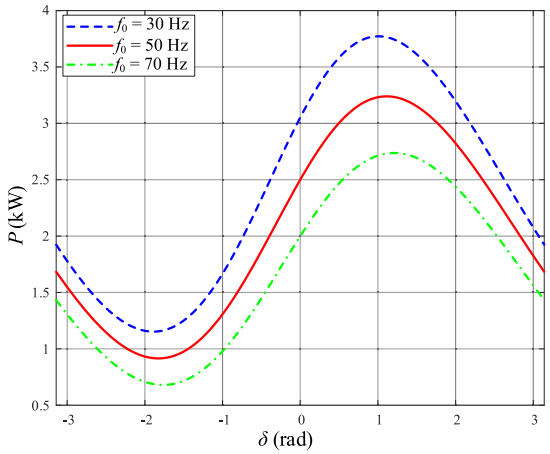

FIGURE 13. *P* - δ **curves with different types of the local load.**

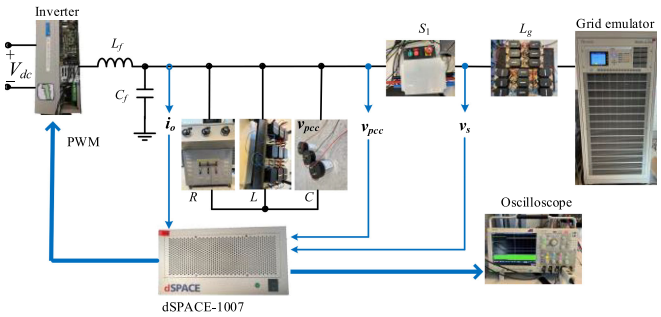

FIGURE 14. Configuration of the experimental setup.

representing a capacitive load. Therefore, it is convenient to emulate different types of the local load by choosing different resonant frequencies f_0.

$$Q_L = \frac{3}{2} \cdot \frac{V^2}{R} \cdot Q_f \left(\frac{f_0}{f_1} - \frac{f_1}{f_0} \right) \tag{17}$$

According to the above explanations, the P - δ curves with different types of local load can be readily plotted based on (9) by setting different f_0. The corresponding P - δ curves are shown in Fig. 13, where $f_0 = 30$ Hz is adopted as an example of the capacitive load and $f_0 = 70$ Hz is selected as an example of the inductive load. From Fig. 13, it is observed that, compared to the case with $f_0 = 50$ Hz, the capacitive or inductive load only makes the P - δ curve move up or down without modifying its shape. Hence, the reconnection of GFM inverters to the grid can still be equivalent to a step change of active power reference. Since the mechanism behind possible loss of synchronism of GFM inverters transitioning from IS to GC mode keeps the same for the different types of local load, all the theoretical analyses and conclusions obtained in the previous parts are still valid for both the capacitive and inductive local loads.

V. EXPERIMENTAL RESULTS

To verify the correctness of the theoretical findings on the transient stability of GFM inverters when transitioning from the IS to GC mode, the experimental tests are conducted, where the configuration of the experimental setup is shown in Fig. 14. The main system parameters listed in Table 1 are used for the experimental setup. The inverter under test is a Danfoss VLT FC-302 frequency inverter, and the power grid is emulated by a Chroma Grid Simulator 61845. The control scheme is implemented in the DS1007 dSPACE system.

In the experimental tests, the GFM inverter initially operates in the IS mode supplying the power to the local load. Then, the resynchronization controller is enabled to resynchronize v_{pcc} with v_s. After that, the STS S_1 is closed to reconnect the GFM inverter with the grid. Since the effectiveness of the adopted resynchronization control scheme has been validated in [11], the experimental waveforms illustrated in the following only show the time periods after the completion of resynchronization to focus on the transient stability of GFM inverters transitioning from the IS to GC mode.

A. VERIFICATION OF IMPACT OF SCR ON THE EXISTENCE OF EQUILIBRIUM POINTS

The impact of the SCR on the existence of EPs is examined first. To emulate different SCRs, $L_g = 6$ mH (i.e., SCR = 4) and $L_g = 24$ mH (i.e., SCR = 1) are selected and tested, respectively. The corresponding experimental waveforms of GFM inverter during transition process are presented in Fig. 15. From Fig. 15(a), after the closure of S_1, the GFM inverter can keep the synchronism with the grid and achieve a smooth transition from the IS to GC mode under the condition of SCR = 4. In contrast, when SCR is reduced to 1, the GFM inverter loses synchronism with the grid after reconnection as shown in Fig. 15(b). Such transient instability is correctly predicted by the P - δ curves in Fig. 7, since there does not exist the EPs after grid reconnection under the case of SCR = 1 when $P_{ref} = 1$ kW. Hence, these experimental results confirm the correctness of the impact of the SCR on the existence of EPs.

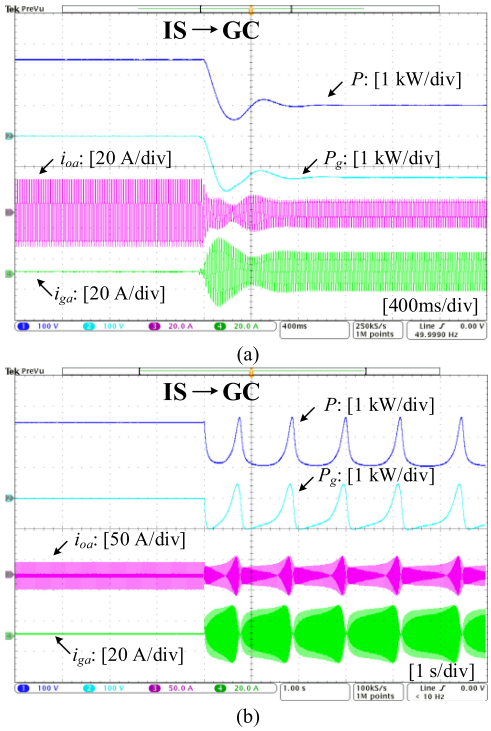

FIGURE 15. When $P_{ref} = 1$ kW, the experimental waveforms of GFM inverter during transition from the IS to GC mode under different SCRs. (a) SCR = 4, (b) SCR = 1.

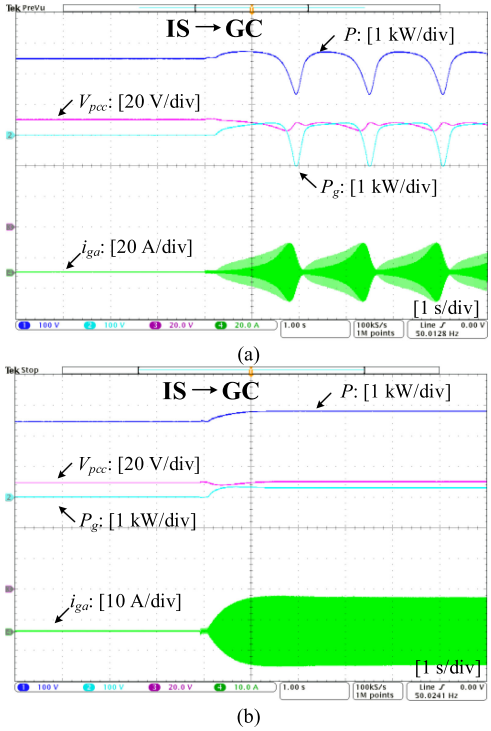

FIGURE 16. When $P_{ref} = 2.8$ kW (the active power is injected into the grid after the reconnection), the experimental waveforms of GFM inverter during transition from the IS to GC mode with (a) the *Q-V* droop control ($K_q = 0.1$ p.u. and $f_c = 0.5$ Hz), (b) the constant voltage magnitude control.

B. VERIFICATION OF THE IMPACT OF Q-V DROOP CONTROL ON THE TRANSIENT STABILITY

Next, the impact of the *Q-V* droop control on the transient stability is tested, where $L_g = 20$ mH is used for the following tests. Based on the theoretical findings, since its impact is dependent on the direction of grid-side active power flow, two scenarios for different grid-side active power flowing directions are emulated, which is realized by setting different active power references for the PSC of the GFM inverter. Besides, the GFM inverter with the constant voltage magnitude control, which is implemented by setting $V = V_0 = 1.0$ p.u., is also tested for the comparison. Firstly, the scenario when the active power is injected into the grid after the reconnection is tested by setting $P_{ref} = 2.8$ kW. The experimental waveforms of the GFM inverter with the *Q-V* droop control during transition process are shown in Fig. 16(a). It is observed that the GFM inverter cannot keep synchronism with the grid after the closure of S_1. In contrast, the experimental waveforms shown in Fig. 16(b) demonstrate that the constant voltage magnitude control guarantees the system transient stability during transition process. The above observations coincide with the phase portraits presented in Fig. 8(a). Hence, the conclusion that the *Q-V* droop control deteriorates the transient stability of GFM inverters when the active power is injected into the grid after the reconnection is verified.

Similarly, the scenario when the active power is extracted from the grid after the reconnection is also tested by setting $P_{ref} = 1.2$ kW, and the corresponding experimental waveforms during transition process are shown in Fig. 17. It is observed that, differing from the previous case, the GFM inverter with the constant voltage magnitude control suffers from the transient instability issue when it is reconnected to the grid as shown in Fig. 17(b). On the contrary, the *Q-V* droop control can enhance the system transient stability and help the GFM inverter keep synchronism with the grid after the closure of S_1 as shown in Fig. 17(a). These experimental results are also in accordance with the phase portraits presented in Fig. 8(b). Consequently, it is proved that the *Q-V* droop control can benefit the transient stability when the active power is extracted from the grid after the reconnection.

C. VERIFICATION OF PARAMETRIC EFFECTS OF POWER CONTROLLERS ON THE TRANSIENT STABILITY

Lastly, the parametric effects of the power controllers on the transient stability are verified, where $L_g = 20$ mH is used and different grid-side active power flowing directions are tested, respectively.

The cutoff frequency f_c of the LPF in the PSC loop is examined first. When $P_{ref} = 1.2$ kW, the experimental waveforms of the GFM inverter with $f_c = 10$ Hz during transition process are presented in Fig. 18(a). It is clear that a stable transition is achieved after the closure of S_1. Nevertheless, when f_c is decreased to 1 Hz, the GFM inverter loses its synchronism with the grid during transition process as shown in Fig. 18(b).

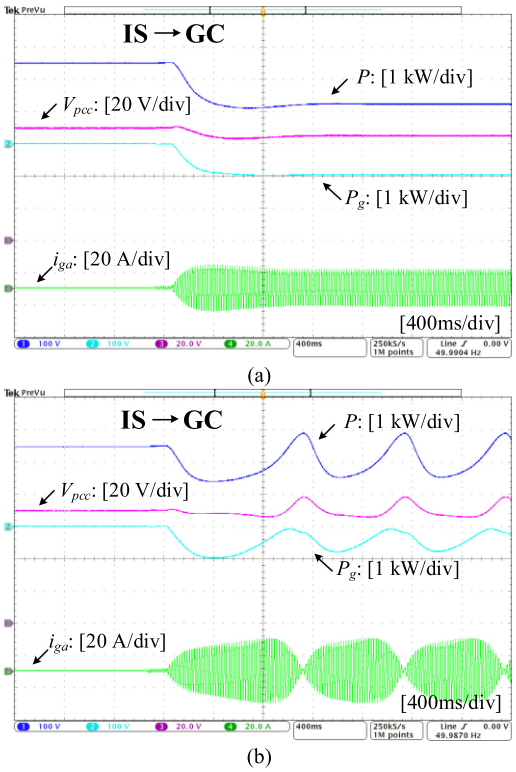

FIGURE 17. When $P_{ref} = 1.2$ kW (the active power is extracted from the grid after reconnection), the experimental waveforms of GFM inverter during transition from the IS to GC mode with (a) the *Q-V* droop control ($K_q = 0.1$ p.u. and $f_c = 2$ Hz), (b) the constant voltage magnitude control.

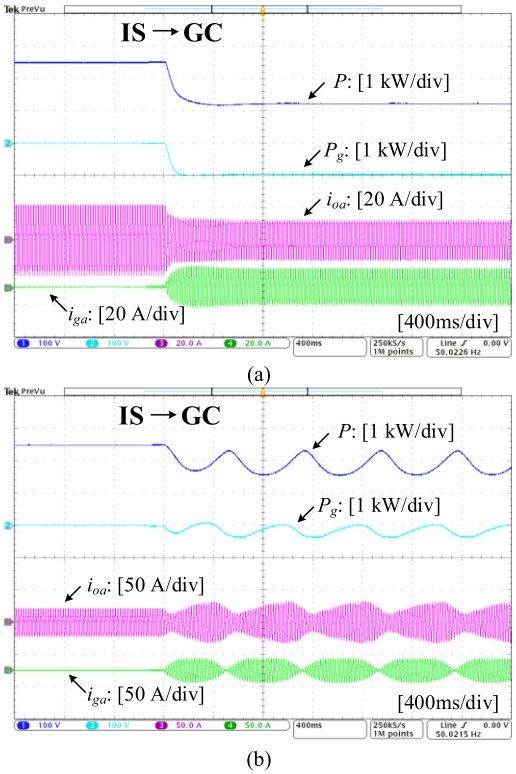

FIGURE 18. When $P_{ref} = 1.2$ kW, the experimental waveforms of GFM inverter during transition from the IS to GC mode with different LPF cutoff frequency f_c of the PSC. (a) $f_c = 10$ Hz and $K_q = 0.1$ p.u., (b) $f_c = 0.5$ Hz and $K_q = 0.1$ p.u.

When the grid-side active power flowing direction is reversed by setting $P_{ref} = 2.8$ kW, the experimental waveforms of the GFM inverter with $f_c = 10$ Hz and $K_q = 0.1$ p.u. during transition process are illustrated in Fig. 19, where a transient stable transition of GFM inverter is observed. Comparing to the case with $f_c = 0.5$ Hz and $K_q = 0.1$ p.u. presented in Fig. 16(a), it is found that the decrease of f_c jeopardizes the system transient stability. Based on the above observations, it is verified that the impact of f_c on the transient stability is independent on the direction of the grid-side active power flow, and the experimental results shown in Figs. 16(a), 18 and 19 coincide with the phase portraits plotted in Fig. 10.

Then, the impact of the *Q-V* droop coefficient under different grid-side active power flowing directions is tested. Fig. 20 shows the experimental waveforms of GFM inverter during transition process when $P_{ref} = 1.2$ kW. From Fig. 20, the GFM inverter can maintain synchronism with the grid after the closure of S_1 with $K_q = 0.2$ p.u. and $f_c = 0.5$ Hz. Comparing to the case with $K_q = 0.1$ p.u. and $f_c = 0.5$ Hz illustrated in Fig. 18(b), where the transient instability occurs during the transition process, it is found that the increase of K_q enhances the system transient stability when the active power is extracted from the grid after the reconnection.

By contrast, when the grid-side active power flowing direction is reversed by setting $P_{ref} = 2.8$ kW, the experimental waveforms of the GFM inverter with $K_q = 0.3$ p.u. and $f_c =$

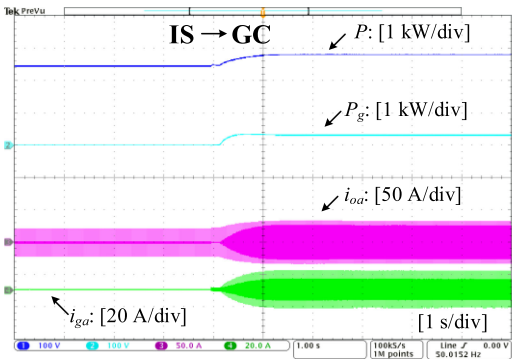

FIGURE 19. When $P_{ref} = 2.8$ kW, the experimental waveforms of GFM inverter during transition from the IS to GC mode with $f_c = 10$ Hz and $K_q = 0.1$ p.u.

10 Hz during transition process are illustrated in Fig. 21. It is clear that the GFM inverter suffers from transient instability after the closure of S_1. Comparing to the case with $K_q = 0.1$ p.u. and $f_c = 10$ Hz presented in Fig. 19, it is confirmed that the increase of K_q deteriorates the system transient stability if the active power is injected into the grid after reconnection, which is opposite to the case when the direction of grid-side active power flow is reversed. The above observations are also in accordance with the phase portraits shown in Fig. 12. Hence, it is verified that the impact of K_q on the transient

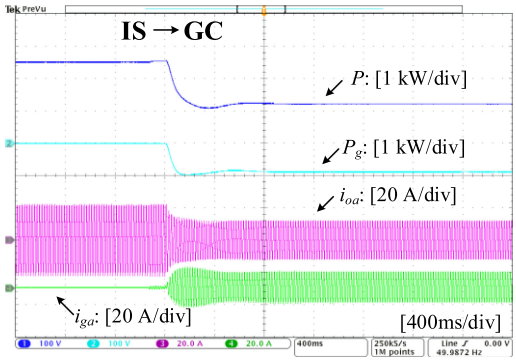

FIGURE 20. When $P_{ref} = 1.2$ kW, the experimental waveforms of GFM inverter during transition from the IS to GC mode with $K_q = 0.2$ p.u. and $f_c = 0.5$ Hz.

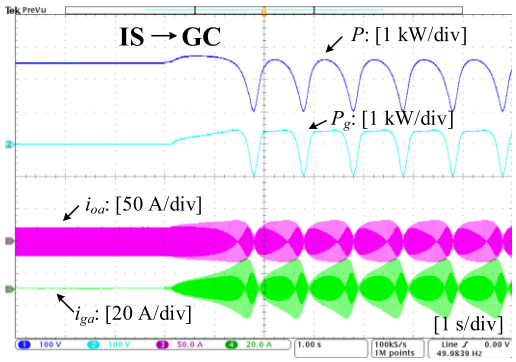

FIGURE 21. When $P_{ref} = 2.8$ kW, the experimental waveforms of GFM inverter during transition from the IS to GC mode with $K_q = 0.3$ p.u. and $f_c = 10$ Hz.

stability is dependent on the grid-side active power flowing direction.

VI. CONCLUSION

This paper presents the transient stability analysis for GFM inverters when transitioning from the IS to GC mode. It has been found out that, although the resynchronization is achieved, the GFM inverter may still lose its synchronism with the grid during the reconnection process. Such reconnection can be equivalent to a step change of the active power reference, where the local load, active power reference of GFM inverter, and the SCR of grid jointly determine its impact on the transient stability after grid reconnection. Next, based on the P - δ curve, it has been revealed that the SCR also has a critical impact on the existence of EPs, where the decrease of SCR makes GFM inverter more prone to the LOS when reconnecting to the grid. Then, through phase portrait-based analysis, it has been found out that the Q-V droop control can enhance the transient stability of GFM inverter if the active power is extracted from the grid after reconnection. In contrast, the Q-V droop control jeopardizes the transient stability when the direction of grid-side active power flow is reversed. Further, the relationship between the parametric effects of power controllers and grid-side active power flow direction has also been identified, which provides a controller design guideline to stably reconnect GFM inverters with the grid. Finally, all the findings have been validated by the experimental results.

REFERENCES

[1] V. Mehr, S. Kahrobaee, and M. Avendano, "Harnessing the full potential of clean energy: The role of southern california's utility distributed energy resource pilots," *IEEE Power Energy Mag.*, vol. 19, no. 4, pp. 28–40, Jul./Aug. 2021.

[2] European Network of Transmission System Operators for Electricity (ENTSO-E), "High penetration of power electronic interfaced power sources and the potential contribution of grid forming converters" *ENTSO-E Tech. Group High Penetration Power Electron. Interfaced Power Sources*, Belgium, Tech. Rep., 2020.

[3] R. H. Lasseter, Z. Chen, and D. Pattabiraman, "Grid-forming inverters: A critical asset for the power grid," *IEEE J. Emerg. Sel. Topics Power Electron.*, vol. 8, no. 2, pp. 925–935, Jun. 2020.

[4] R. Rosso, X. Wang, M. Liserre, X. Lu, and S. Engelken, "Grid-forming converters: Control approaches, grid-synchronization, and future Trends—A review," *IEEE Open J. Ind. Appl.*, vol. 2, pp. 93–109, 2021.

[5] *GC0137: Minimum Specification Required for Provision of GB Grid Forming Capability (formerly Virtual Synchronous Machine Capability)*, National Grid Code, Feb. 2021.

[6] Q. Zhong and G. Weiss, "Synchronverters: Inverters that mimic synchronous generators," *IEEE Trans. Ind. Electron.*, vol. 58, no. 4, pp. 1259–1267, Apr. 2011.

[7] J. W. Simpson-Porco, F. Dörfler, and F. Bullo, "Synchronization and power sharing for droop-controlled inverters in islanded microgrids," *Automatica*, vol. 49, no. 9, pp. 2603–2611, 2013.

[8] M. Karimi-Ghartemani, "Universal integrated synchronization and control for single-phase DC/AC converters," *IEEE Trans. Power Electron.*, vol. 30, no. 3, pp. 1544–1557, Mar. 2015.

[9] *IEEE Standard for Interconnection and Interoperability of Distributed Energy Resources with Associated Electric Power Systems Interfaces*, IEEE Std 1547-2018 (Revision of IEEE Std 1547-2003), Apr. 2018.

[10] Y. A. I. Mohamed and A. A. Radwan, "Hierarchical control system for robust microgrid operation and seamless mode transfer in active distribution systems," *IEEE Trans. Smart Grid*, vol. 2, no. 2, pp. 352–362, Jun. 2011.

[11] Y. Li, D. M. Vilathgamuwa, and P. C. Loh, "Design, analysis, and real-time testing of a controller for multibus microgrid system," *IEEE Trans. Power Electron.*, vol. 19, no. 5, pp. 1195–1204, Sep. 2004.

[12] M. Ramezani, S. Li, F. Musavi, and S. Golestan, "Seamless transition of synchronous inverters using synchronizing virtual torque and flux linkage," *IEEE Trans. Ind. Electron.*, vol. 67, no. 1, pp. 319–328, Jan. 2020.

[13] C. Verdugo, J. I. Candela, and P. Rodriguez, "Re-synchronization strategy for the synchronous power controller in HVDC systems," in *Proc. IEEE Energy Convers. Congr. Expo.*, Cincinnati, OH, USA, 2017, pp. 5186–5191.

[14] M. Amin and Q. Zhong, "Resynchronization of distributed generation based on the universal droop controller for seamless transfer between operation modes," *IEEE Trans. Ind. Electron.*, vol. 67, no. 9, pp. 7574–7582, Sep. 2020.

[15] V. L. Srinivas, B. Singh, and S. Mishra, "Seamless mode transition technique for virtual synchronous generators and method thereof," *IEEE Trans. Ind. Inform.*, vol. 16, no. 8, pp. 5254–5266, Aug. 2020.

[16] V. L. Srinivas, B. Singh, and S. Mishra, "Self-synchronizing VSM with seamless operation during unintentional islanding events," *IEEE Trans. Ind. Inform.*, vol. 16, no. 9, pp. 5680–5690, Sep. 2020.

[17] X. Wang, M. G. Taul, H. Wu, Y. Liao, F. Blaabjerg, and L. Harnefors, "Grid-synchronization stability of converter-based resources—An overview," *IEEE Open J. Ind. Appl.*, vol. 1, pp. 115–134, 2020.

[18] H. Wu and X. Wang, "Design-oriented transient stability analysis of grid-connected inverters with power synchronization control," *IEEE Trans. Ind. Electron.*, vol. 66, no. 8, pp. 6473–6482, Aug. 2019.

[19] X. Fu *et al.*, "Large-signal stability of grid-forming and grid-following controls in voltage source inverter: A comparative study," *IEEE Trans. Power Electron.*, vol. 36, no. 7, pp. 7832–7840, Jul. 2021.

[20] D. Pan, X. Wang, F. Liu, and R. Shi, "Transient stability of voltage-source inverters with grid-forming control: A design-oriented study," *IEEE J. Emerg. Sel. Topics Power Electron.*, vol. 8, no. 2, pp. 1019–1033, Jun. 2020.

[21] T. Liu and X. Wang, "Transient stability of single-loop voltage-magnitude controlled grid-forming inverters," *IEEE Trans. Power Electron.*, vol. 36, no. 6, pp. 6158–6162, Jun. 2021.
[22] L. Huang, H. Xin, Z. Wang, L. Zhang, K. Wu, and J. Hu, "Transient stability analysis and control design of droop-controlled voltage source inverters considering current limitation," *IEEE Trans. Smart Grid*, vol. 10, no. 1, pp. 578–591, Jan. 2019.
[23] H. Xin, L. Huang, L. Zhang, Z. Wang, and J. Hu, "Synchronous instability mechanism of *P-f* droop-controlled voltage source inverter caused by current saturation," *IEEE Trans. Power Syst.*, vol. 31, no. 6, pp. 5206–5207, Nov. 2016.
[24] N. Soni, S. Doolla, and M. C. Chandorkar, "Improvement of transient response in microgrids using virtual inertia," *IEEE Trans. Power Del.*, vol. 28, no. 3, pp. 1830–1838, Jul. 2013.
[25] J. Alipoor, Y. Miura, and T. Ise, "Stability assessment and optimization methods for microgrid with multiple VSG units," *IEEE Trans. Smart Grid*, vol. 9, no. 2, pp. 1462–1471, Mar. 2018.
[26] M. H. Roos, P. H. Nguyen, J. Morren, and J. G. Slootweg, "Modeling and experimental validation of power electronic loads and DERs for microgrid islanding simulations," *IEEE Trans. Power Syst.*, vol. 35, no. 3, pp. 2279–2288, May 2020.
[27] J. D. Rios Penaloza, J. A. Adu, A. Borghetti, F. Napolitano, F. Tossani, and C. A. Nucci, "Influence of load dynamic response on the stability of microgrids during islanding transition," *Electron. Power Syst. Res.,* vol. 190, Jan. 2021, Art. no. 106607.
[28] Y. Gu, N. Bottrell, and T. C. Green, "Reduced-order models for representing inverters in power system studies," *IEEE Trans. Power Electron.*, vol. 33, no. 4, pp. 3645–3654, Apr. 2018.
[29] S. H. Strogatz. *Nonlinear Dynamics and Chaos: With Applications to Physics, Biology, Chemistry, and Engineering*. New York, NY, USA: Perseus Books, 1994.
[30] M. G. Taul, X. Wang, P. Davari, and F. Blaabjerg, "An overview of assessment methods for synchronization stability of grid-connected inverters under severe symmetrical grid faults," *IEEE Trans. Power Electron.*, vol. 34, no. 10, pp. 9655–9670, Oct. 2019.

TENG LIU (Member, IEEE) received the B.S. and Ph.D. degrees in electrical engineering from Xi'an Jiaotong University, Xi'an, China, in 2012 and 2019, respectively. He is currently a Postdoc with AAU Energy, Aalborg University, Aalborg, Denmark. His current research focuses on modeling, control, and stability analysis of grid-connected converters. He was the recipient of the MPCE Excellent Reviewer Award in 2020.

XIONGFEI WANG (Senior Member, IEEE) received the B.S. degree in electrical engineering from Yanshan University, Qinhuangdao, China, in 2006, the M.S. degree in electrical engineering from the Harbin Institute of Technology, Harbin, China, in 2008, and Ph.D. degree in energy technology from Aalborg University, Aalborg, Denmark, in 2013. Since 2009, he has been with the Department of Energy, AAU Energy Aalborg University, where he was an Assistant Professor in 2014, an Associate Professor in 2016, and a Professor and the Leader of Electronic Power Grid Research Group in 2018. From 2020, he has also been a Part-Time Professor with the KTH Royal Institute of Technology, Stockholm, Sweden. His current research interests include modeling and control of power electronic converters and systems, stability and power quality of power-electronics-dominated power systems, high-power converters. He is the Co-Editor-in-Chief for the IEEE TRANSACTIONS ON POWER ELECTRONICS and an Associate Editor for the IEEE JOURNAL OF EMERGING AND SELECTED TOPICS IN POWER ELECTRONICS. He was the recipient of nine Prize Paper Awards in the IEEE Transactions and conferences, the 2016 AAU Talent for Future Research Leaders, the 2018 Richard M. Bass Outstanding Young Power Electronics Engineer Award, the 2019 IEEE PELS Sustainable Energy Systems Technical Achievement Award, the 2020 IEEE PES Prize Paper Award, the 2020 JESTPE Star Associate Editor Award, the 2022 Isao Takahashi Power Electronics Award, and the Highly Cited Researcher in the Web of Science from 2019.

FANGCHENG LIU (Senior Member, IEEE) received the B.S. degree in electrical engineering from the Huazhong University of Science and Technology, Wuhan, Chinaand the Ph.D. degree in electrical engineering from Xi'an Jiaotong University, Xi'an, China, in 2007 and 2014, respectively.

Since 2014, he has been with Huawei, Shenzhen, China, where he is currently the Principal Engineer with Digital Power Technology & Strategy Dept (Part of Huawei Digital Power Technologies). His research interests include modeling and control of grid-connected converters, and stability of power electronic based power systems.

KAI XIN received the Ph.D. degree in electrical engineering from Huazhong University of Science and Technology, Wuhan, China in 2007. From 2007 to 2011, he was a Researcher with Power Conversion System Control Lab, General Electric Global Research Center, Shanghai, China. Since 2011, he has been with Huawei, where he is currently a Technical Expert with Power Electronics Technology Lab (Part of Huawei Digital Power Technologies). His research interests include grid-connected PV/wind power generation system and energy conversion techniques and applications.

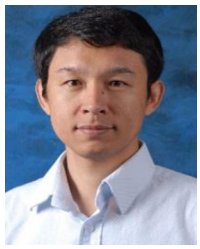

YUNFENG LIU received the Ph.D. degree in electronic engineering from Southeast University, Nanjing, China, in 1999.

From 1999 to 2001, he was a Postdoctoral Researcher with the Department of Electrical Engineering, Tsinghua University, Beijing, China. From 2001 to 2003, he was a Visiting Scholar with the Center for Power Electronics Systems, Virginia Tech, Blacksburg, VA, USA. From 2003 to 2011, he was a Senior Researcher with General Electric Global Research Center (GE GRC), Shanghai, China and a Manager with Power Conversion System Control Lab, GE GRC. Since 2011, he has been with Huawei, Shenzen, China, where he is currently the Chief Scientist with Huawei Digital Power Technologies Co. Ltd. His research interests include high power semiconductor devices, converter and application in power system, and energy conversion techniques and applications.